THE JOURNAL OF PHYSICAL CHEMISTRY C
A JOURNAL OF THE AMERICAN CHEMICAL SOCIETY

pubs.acs.org/JPCC Article

Cu(II)–Glycerol–*N*-Ethylmorpholine Complex Stability Revealed by X-ray Spectroscopy

Giovanni La Penna, Fabrizio Machetti, Olivier Proux, Giancarlo Rossi, Francesco Stellato, and Silvia Morante*

Cite This: https://dx.doi.org/10.1021/acs.jpcc.0c08676 Read Online

ACCESS | Metrics & More | Article Recommendations | Supporting Information

ABSTRACT: We report on a detailed X-ray absorption spectroscopy study of the Cu(II) coordination mode in aqueous solution in the presence of glycerol cryoprotectant and *N*-ethylmorpholine buffer. The first additive is often used when working at very low temperatures with the purpose of avoiding unwanted ice diffraction, the second is used to allow adjusting the pH at the desired value. Additives of this kind are routinely used in experiments. It is thus mandatory to have a precise understanding of their structural interaction with metals and in particular with Cu, which is among the most important protein-binding ions, in order to identify spurious spectral signatures in the X-ray spectrum of metal–protein complexes possibly polluting the collected data. Our XAS data show that the spectrum of Cu in the presence of these additives is significantly different from that of Cu in pure water, thus suggesting a direct interaction of glycerol and *N*-ethylmorpholine with the metal ion. Classical and *ab initio* numerical simulations are employed to construct structural models of the metal environment able to reproduce the features of the measured X-ray spectrum. In particular, starting from system configurations extracted from classical molecular dynamics simulations, we have successively refined their geometrical structure by optimizing the local Cu binding site by DFT relaxation runs. The fit to the experimental data obtained from the initial geometrical parameters of the Cu binding site determined in this way is very good and shows that both glycerol and *N*-ethylmorpholine contribute to the Cu coordination.

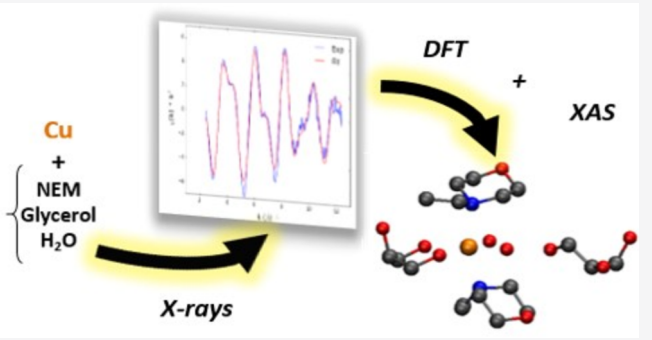

INTRODUCTION

X-ray absorption spectroscopy (XAS) allows for investigation of metals in almost any system in any state (solid, liquid, gaseous). Thus, it can be profitably used for structural studies of biological systems. In particular, XAS is a largely employed technique for investigating the metal local environment in metal–protein complexes in solution at physiological conditions. Moreover, XAS is useful when dealing with unstructured and intrinsically disordered proteins (IDPs) where other techniques of structural biology, such as X-ray diffraction and NMR, provide only partial information.

It is well-known that biological samples are prone to photodamage under X-ray irradiation.[1] In order to mitigate radiation damage at X-ray sources, experiments are usually performed at low temperature (~10–15 K). However, in these conditions ice diffraction by the frozen microcrystalline water molecules can become a nuisance since it can generate spurious signals superimposed to the proper sample XAS signal. This problem is often addressed by adding glassing agents (such as glycerol or ethylene glycol) to the solution, thus obtaining an ice-free glass upon rapid freezing in liquid nitrogen. Other interesting possibilities are discussed in ref 2.

Keeping the pH at the desired value is also a very important issue, as a protein may undergo a reorganization of its three-dimensional structure in response to pH modifications. In fact, pH changes affect electrostatic interactions between charged amino acid functional groups, consequently altering the binding of the protein to metal ions.[3] The pH value can be held fixed (or at least kept in a controlled range) by adding an appropriate buffer to the solution.

Actually controlling pH and ionic force *in vitro* is an issue of more general interest, relevant in the case of sample preparation for microscopy and macromolecular imaging.[4]

Noticeable effects of the buffer choice are also seen in studies of IDPs, a paradigmatic example of which is represented by the case of the amyloid-β (Aβ) peptide involved in Alzheimer's disease.[5] The value of the Cu–Aβ

Received: September 23, 2020
Revised: December 29, 2020

dissociation constant is influenced by the buffer choice, because of the combined effect of the Cu affinity for the buffer conjugate base (B) and the formation of the ternary complex B−Cu−Aβ.[6−8] The Cu−Aβ binding mode depends on pH and is highly fluxional. Buffer choice affects not only XAS measurements[9] but also ESR spectroscopy.[10−12] In particular, the *N*-ethylmorpholine (NEM) buffer is used to reduce the ESR signal of aqueous Cu(II) complexes,[13,14] while no interference is observed in the Cu−Aβ binding formation.[15] Owing to these properties the NEM buffer is widely used when metal-binding proteins are investigated.[16]

For the reasons discussed above (i.e., to prevent ice formation upon rapid freezing and the need to adjust the system pH at the desired value), biological samples undergoing XAS measurements as well as other spectroscopies are usually solvated in a mixture containing both a cryoprotectant (such as glycerol) and a buffer (such as NEM).[14,16−20] [We are aware of the fact that other buffers, for instance PBS (phosphate-buffered saline) and HEPES (4-(2-hydroxyethyl)-1-piperazineethanesulfonic acid), are also used (see https://en.wikipedia.org/wiki/Good%27s_buffers), but in this paper we will be limited to consideration of the specific case where NEM is employed.]

The study we present is based on a synergistic combination of XAS measurements and computational techniques, and it is aimed at understanding the structure of the local environment around Cu(II) ions in an aqueous solution containing both cryoprotectant and buffer molecules.

The main result of this investigation is that the XAS spectrum of Cu in water in the presence of glycerol and NEM shows features (especially visible in the Fourier transform (FT) of the EXAFS region of the spectrum) that can only be explained by assuming that both additives are coordinated to the metal.

One might think that this coordination is anyway not going to affect the XAS signal in the case of a protein−metal complex, because the Cu binding constants of proteins are typically larger than those of molecules such as glycerol and NEM. However, two observation are in order here. First, we should recall that additives are present in solution at a much higher concentration (from 100 to 1000 times) than that of the protein. Second, as suggested in ref 6 in the specific case of Aβ peptides, Cu(Aβ)L complexes are formed where buffer molecules represent the ligand components "L". Thus, since additives could act as first-shell additional ligands contributing to the intensity of the measured XAS signal with peculiar (and unwanted) spectral features, we believe that providing structural information on the way glycerol and NEM can coordinate to Cu is an important issue worth investigating.

In closing this introductory section we wish to stress that the case we are studying in this paper can be of relevance in other similar situations as it represents a paradigmatic example of the role that additives can play in the emerging field of investigation regarding the interaction between metal ions and proteins, especially the intrinsically disordered class.

MATERIAL AND METHODS

In order to study how the Cu coordination site is affected by the presence of glycerol and NEM, we compare the XAS spectra of Cu in aqueous solutions in the presence and in the absence of these two additives.

Sample Preparation. We have prepared different samples containing Cu(II) ions in various solution conditions. In a first sample (denoted by S_1 in the following) 10 mM $CuSO_4$ is dissolved in high-purity water, while in a second sample (denoted by S_2) 2 mM $CuSO_4$ is dissolved in water containing 50% (v/v) glycerol and 100 mM NEM buffer. We have also prepared a further sample in which 2 mM $CuSO_4$ is dissolved in water plus 50% (v/v) glycerol. [The 2 mM concentration of $CuSO_4$ in S_2 was chosen because this is the typical concentration in which peptides are commonly dissolved. On the other hand, in order to reduce the acquisition time of the S_1 XAS spectrum, the concentration of $CuSO_4$ in pure water was taken to be 10 mM. We have however checked that, in the range we considered, i.e., 2−10 mM, the Cu concentration does not affect the metal coordination mode in water and that not even in the case of the largest Cu concentration are self-absorption effects appreciable (data are shown in Figure 1 of the Supporting Information).]

In all samples, the solution was kept at pH 7.4 by rapidly adding, before the addition of glycerol, the appropriate amount of sulfuric acid to prevent the formation of copper precipitates in the presence of NEM. The details of the pH calibration are described in the Supporting Information.

For sample preparations Milli-Q water was used throughout, together with glycerol (99.5%, Aldrich), *N*-ethylmorpholine (99.0%, TCI), copper sulfate anydrous (99.99%, Aldrich), and sulfuric acid (95−97%, Fluka). All compounds were used as supplied.

XAS Data Collection. XAS experiments on the S_1 and S_2 samples were carried out at the BM30B beamline of the European Synchrotron Radiation Facility (ESRF, Grenoble, France).[21] The beam energy was selected using a Si(220) double-crystal monochromator with a resolution of 0.5 eV. The beam spot on the sample was approximately 300 × 200 μm^2 ($H \times V$, fwhm). Spectra were recorded in fluorescence mode by using a 30-element solid state Ge detector. To minimize photodegradation and spectra evolution during XAS measurements, all the samples were first rapidly brought from room temperature to 77 K and then cooled and kept at 13 K in a liquid helium cryostat. For the same reason in the process of data acquisition, samples were systematically moved to a different position after each scan.

The photon energy was calibrated with a Cu foil used as a standard, setting the maximum of the first derivative of the spectrum at 8979 eV. The XAS data of the S_1 sample were obtained as the average of three separate scans, while S_2 data resulted from averaging over six scans. Each scan lasted about 30 min. In view of the dimension of the beam, samples were moved, along the vertical direction, by about 400 μm after each scan. Individual scans of S_1 and S_2 are shown in Figures 3 and 4 of the Supporting Information. Data from different scans appear perfectly well superimposable.

The XANES spectra were normalized by use of the software Athena.[22] EXAFS data were extracted by using cubic splines as implemented in the AUTOBKG algorithm[23] of Athena. The subsequent quantitative data analysis was performed by using the program EXCURV98.[24]

XAS Data Analysis. To be able to reliably determine the Cu atomic environment from a structural fit of the experimental XAS data, a number of possible structures were produced with the help of classical molecular dynamics (MD) simulations and refined by successive DFT relaxation runs (details of this computational process are given in Classical Molecular Dynamics Simulations and Structural Models and DFT Relaxation). The structural parameters obtained in this

https://dx.doi.org/10.1021/acs.jpcc.0c08676
J. Phys. Chem. C XXXX, XXX, XXX−XXX

way are used for the fitting of the EXAFS (extended X-ray absorption fine structure) region of the spectrum, while monitoring the shape of the XANES region of the spectrum allows us to follow the evolution of the metal oxidation state.

Classical Molecular Dynamics Simulations. We have built three structural coordination models of the metal site for Cu(II):

(1) in water

(2) in a glycerol/NEM/water matrix

(3) in a glycerol/water mixture

The geometries of these coordination models are the result of an elaborated computational process based on the simulation of empirically parametrized structures, as we are now going to detail.

Models of the Cu(II) coordination mode in pure water (model 1) are constructed following the strategy discussed in ref 25. To build the Cu(II) coordination site in a glycerol/NEM/water matrix (model 2), we had to start from the construction of the Cu site in a glycerol/water mixture (model 3). Many studies are reported in the literature about this kind of system, owing to its relevance as a model of hydrogen bond modulation in liquids.[26] Following recent literature,[27] we began by building an empirical model of a sample of glycerol/water mixture at 20% in volume. This initial mixture corresponds to about 16 water molecules per glycerol molecule.

A cubic lattice of 9 × 9 × 9 glycerol molecules was created with a spacing suitable to span a cubic cell with a 9 nm side.

Every glycerol molecule was initially set in an *all-trans* conformation. The box was then filled with water molecules by using the SOLVATE plugin of VMD,[28] by assembling smaller cubic cells with a 1.8774 nm side containing water molecules taken from a TIP3P[29] simulation at the standard density of 1 g/cm^3. The resulting system (729 glycerol molecules plus 11 457 water molecules) has a water/glycerol fraction equal to 15.7, approximately corresponding to an initial 20% glycerol/water mixture.

The glycerol force field we used was the one extensively employed in the literature in other MD simulations.[27,30] The system was equilibrated in the *NpT* ensemble with temperature and pressure fixed at T = 300 K and p = 0.1 MPa, respectively, for 1 ns.

Systems with a 50% glycerol/water mixture, which corresponds to having four water molecules for each glycerol molecule, were also constructed in order to obtain a glycerol concentration near that of the measured sample, S_2. This concentration was obtained starting from a 20% glycerol/water solution by successively deleting randomly chosen water molecules while at the same time consistently reducing the cell size.

Every time the system composition and the cell size were changed, a 1 ns *NpT* equilibration step was performed. Using this procedure, we have constructed for our further studies two 50% glycerol/water mixture simulation boxes: a large box system (LBS) composed by 510 glycerol molecules and 2021 water molecules and a small box system (SBS) composed by 182 glycerol molecules and 721 water molecules.

To check the reliability of the above construction, we have performed 10 successive MD simulation runs of the 50% glycerol/water mixture, with a step of 30 K, in a temperature range between 200 and 400 K, and compared the resulting glycerol/water density as a function of temperature with the experimental and simulation data of ref 27. The simulations were carried out with the LAMMPS code[31] using the same setting as in ref 27.

The agreement with the published experimental and simulation data is rather good as one can see from Figure 1, where we plot our points (red solid circles), together with the experimental data (green open circles) and the simulation results of ref 27 (blue solid squares).

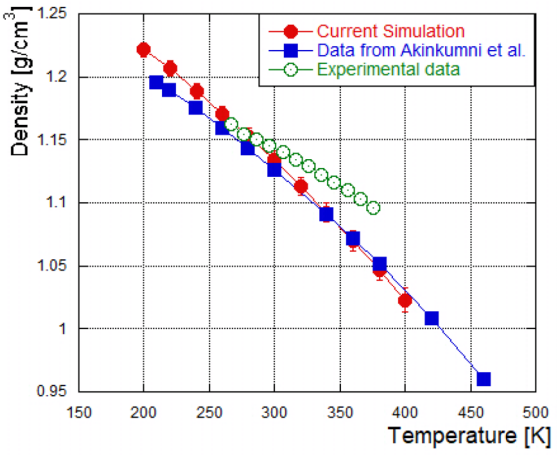

Figure 1. Density (g/cm^3) of the 50% glycerol/water mixture as a function of temperature. Red solid circles are our simulation data. Green open circles are the experimental data. Blue solid squares are simulation data from ref 27.

The last configuration of the equilibrated glycerol/water system obtained at T = 300 K was then used to build up the systems of interest by inserting in it either Cu (obtaining Cu in a glycerol/water mixture, model 3) or Cu plus NEM molecules (obtaining Cu in a glycerol/NEM/water matrix, model 2), as we are now going to describe.

For the insertion of Cu in the glycerol/water matrix, the SBS was used. The insertion of Cu and NEM molecules into the glycerol/water matrix was carried out instead in the LBS to allow for several NEM molecules to be accommodated in the box.

At variance with the case of Cu(II) in water, where a regular octahedral site for Cu(II) was used,[32] in the case of the glycerol/water mixture Cu(II) ions are inserted in a distorted octahedral geometry. This distortion, which is a physically relevant feature largely recognized in recent studies,[33] is forced on the Cu(II)−water environment by (a slightly modified version of) the "dummy" atom method.[32,34−37]

The Cu ion is placed at the center of the SBS simulation box. This system is then equilibrated for 1 ns in the *NpT* ensemble. During equilibration, electrostatic interactions with water molecules and glycerol O atoms are rapidly formed and the Cu ion becomes trapped into a distorted binding site. We have checked that already after 0.5 ns the geometrical structure of the metal binding site does not appreciably change anymore.

The insertion of Cu and NEM molecules into the glycerol/water matrix (aimed at preparing model 2) was carried out in the LBS to allow, as we said, for several NEM molecules to be accommodated in the box so as to have a NEM concentration comparable with the one of the S_2 sample. To insert Cu and NEM molecules in the glycerol/water mixture at 50% volume ratio, the first step was to place a Cu ion together with two

https://dx.doi.org/10.1021/acs.jpcc.0c08676
J. Phys. Chem. C XXXX, XXX, XXX−XXX

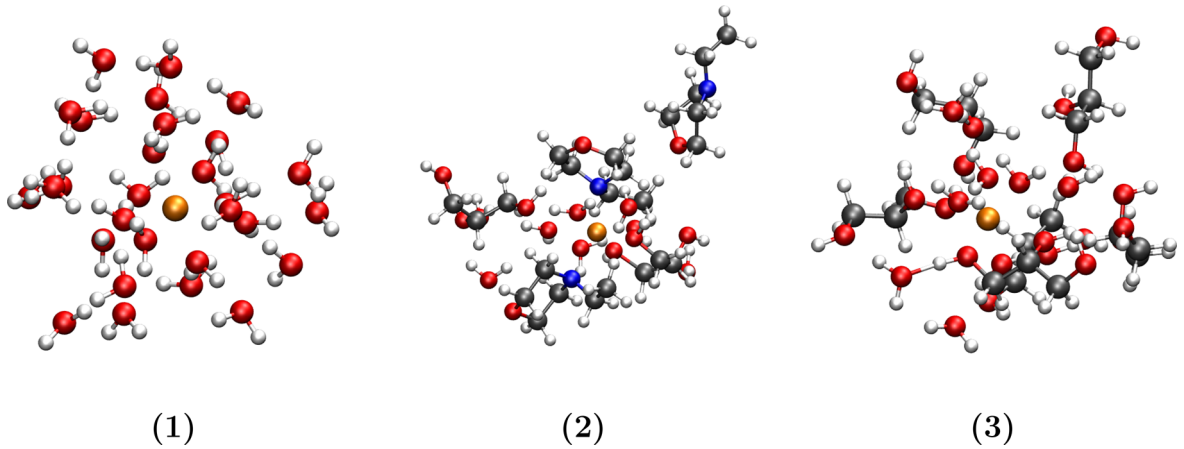

Figure 2. Sketch of the configurations chosen to undergo DFT relaxation. 1, Cu(II) in pure water; 2, Cu(II)−NEM compound inspired by the structure of the ACMRCU10 complex in a 50% glycerol/water mixture; 3, Cu(II) in a glycerol/water 50% mixture. Color code is as follows: C, gray; H, white; O, red; N, blue; and Cu, orange. Bond and atomic radii are depicted only to guide the eye. VMD software[28] was used to generate the drawings.

NEM molecules at binding distance, at the center of the simulation box. The configuration of the Cu−NEM complex is inspired by the structure of the bis(acetato-*O*)-bis-(morpholine)−copper(II) dihydrate complex deposited in the Cambridge Structural Database (CSD)[38] under the code CCDC 1100799 (ACMRCU10).[39,40]

In the ACMRCU10 structure Cu is coordinated to the two N atoms of the two morpholine rings. They have Cu in the same arrangement with the Cu−N bond lying in the ring equatorial plane. Notwithstanding this initial arrangement, during the simulation at room conditions the bonds around N(NEM) can change orientation, with the Cu−N bond moving to an axial direction with respect to the morpholine ring plane. It is important to stress that, in our models, Cu is never covalently bound to NEM by harmonic potentials; nevertheless rather "strong" electrostatic interactions exist that roughly approximate binding potentials.

Besides the two Cu-related NEM molecules mentioned above, six more NEM molecules are (randomly) inserted in the box. With this number we obtain a NEM concentration near the value used in our XAS measurements on the S_2 sample, which is 100 nM.

The OPLS-AA[41] functional form, which was successfully employed in similar simulations of morpholine and morpholine derivatives,[42] was used to parametrize the NEM force field.

After equilibration, a 1 ns simulation in the *NpT* ensemble of the whole Cu + 50% glycerol/water + NEM mixture was performed at T = 300 K. Typical configurations identified along the simulation trajectory were chosen as representative candidates of the Cu−NEM binding mode for our subsequent analysis.

Structural Models and DFT Relaxation. The main goal of this investigation is to understand the features of the X-ray spectrum of Cu(II) in the presence of a glycerol/NEM/water matrix and in particular to explain the existence at about 3.3 Å of an unmistakable bump in the FT of the EXAFS region clearly visible in Figure 3c below. We will show that in the absence of NEM molecules no such feature can be borne out in the spectra of the simulated model systems.

In order to elucidate this issue, we need to compare the EXAFS spectra generated by the geometrical structure of the binding site that Cu(II) acquires in model systems where NEM is absent (models 1 and 3) with what one gets when NEM is added to Cu immersed in a 50% glycerol/water mixture (model 2).

All the above model systems are constructed starting from equilibrated MD configurations. In order to test the reliability and the stability of the configurations generated by classical simulations, we have subjected representative structures of portions of the simulation box that include the first two Cu(II) coordination shells (more precisely all the molecules having at least one atom at a distance not larger than 5.5 Å from the metal) to a DFT optimization run. Consideration of reduced systems of this kind is enough for our analysis, since atoms located at distances larger than this cutoff radius do not contribute to the appearance of the peak at about 3.3 Å in the FT of the S_2 EXAFS region of the spectrum. DFT relaxation is a necessary step to overcome possible instability problems ensuing from the use of empirically parametrized forces, in particular of the dummy atom method we employed to force the correct geometry of the Cu(II)−water environment. DFT is a robust and reliable tool, especially for this goal, which is widely used for large atomic systems (with 100−1000 atoms) like ours.

The structures of the Cu environment of samples 1, 2, and 3 resulting from this construction, prior to DFT optimization, are sketched in Figure 2.

For DFT relaxation we have used the parallel version of the Quantum-Espresso package (version 6.3)[43] where Vanderbilt ultrasoft pseudopotentials[44] and the PBE exchange−correlation functional[45] are implemented. Electronic wave functions have been expanded in plane waves up to an energy cutoff of 25 Ry, while a 300 Ry cutoff was used for the expansion of the augmented charge density in the proximity of the atoms, as required in the ultrasoft pseudopotential scheme. The atoms belonging to the first two Cu(II) coordination shells are inserted into a cubic supercell with sides equal to 24 Å, i.e., large enough to avoid interactions among the system periodic images. After a number (from 50 to 150) of steps of energy minimization, performed with the Broyden−Fletcher−Goldfarb−Shanno algorithm, the atomic forces come to have components never larger than 0.01 Ry/bohr.

The DFT relaxation was performed with spin-polarized Kohn−Sham (KS) monoelectronic states within the local spin

https://dx.doi.org/10.1021/acs.jpcc.0c08676
J. Phys. Chem. C XXXX, XXX, XXX−XXX

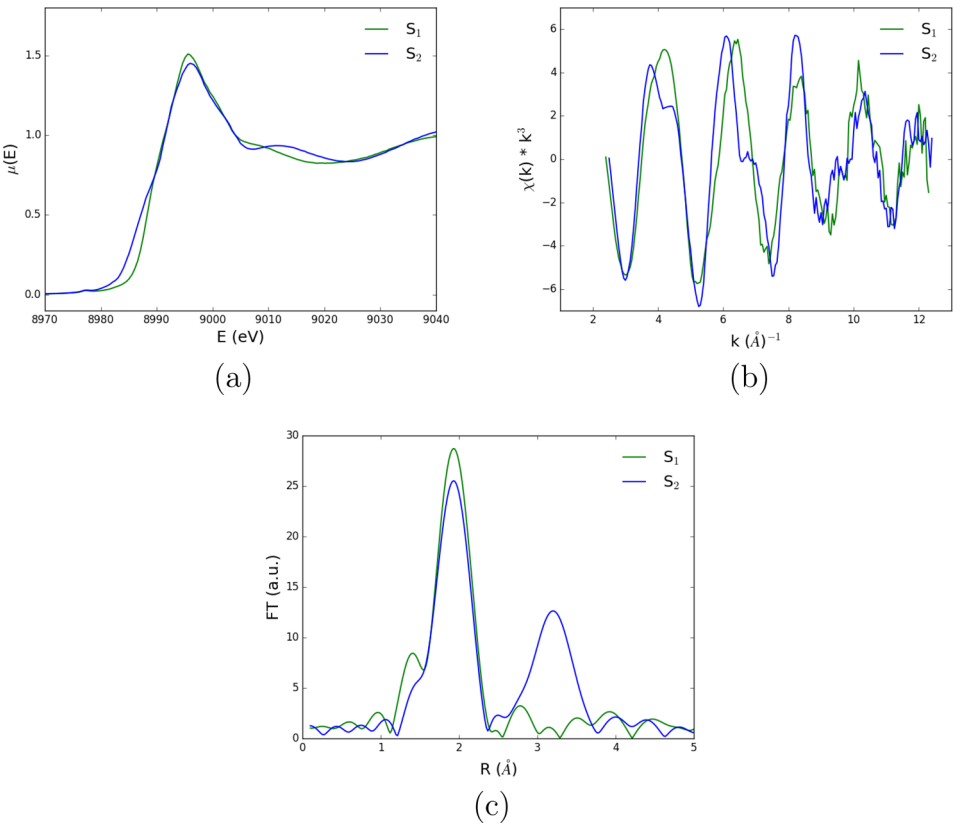

Figure 3. Comparison between S_1 and S_2 systems. Green curves, S_1 system (10 mM $CuSO_4$ in pure water). Blue curves, S_2 system (2 mM $CuSO_4$ + 50% (v/v) glycerol + 100 mM NEM). (a) XANES region. (b) EXAFS region. (c) EXAFS region Fourier transform.

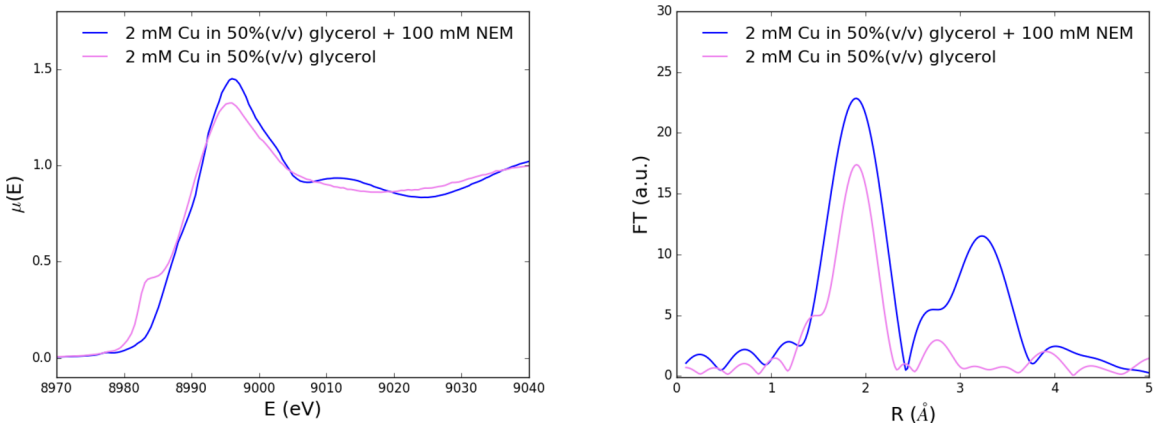

Figure 4. Comparison between XAS data of the S_2 system (in blue) with the data of a system consisting of 2 mM $CuSO_4$ in 50% (v/v) glycerol (in purple). Left panel: XANES data. Right panel: Fourier transform of EXAFS data.

density approximation (LSDA). In all calculations the expectation value of the z component of the spin operator was taken equal to 1/2. An implicit solvent was used to account for the dielectric permittivity at distances larger than 5.5 Å from Cu, mimicking the bulk liquid water environment. The Environ 1.0 module of Quantum-Espresso was employed[46] to model the implicit solvent in DFT plane-wave calculations.

We do not show the resulting DFT relaxed configurations because they are graphically indistinguishable from the ones drawn in Figure 2. To get an idea of the magnitude of their tiny difference, however, we computed the values of the root-mean-square deviations (excluding H atoms) of the initial configurations with respect to the final ones, finding 0.49, 0.51, and 0.18 Å for models 1, 2, and 3, respectively. Most of the contribution to these small numbers comes from the displacement of the Cu ion in an environment that does not change appreciably during the DFT relaxation.

RESULTS AND DISCUSSION

We start our analysis by qualitatively comparing in Figure 3a the XANES region of the measured Cu(II) spectrum in pure water (system S_1) with that of Cu(II) in the presence of glycerol and NEM (system S_2). In Figure 3b we extend the comparison to the EXAFS region. We observe that in both regions the green (S_1 system) and blue (S_2 system) curves are

https://dx.doi.org/10.1021/acs.jpcc.0c08676
J. Phys. Chem. C XXXX, XXX, XXX−XXX

significantly different, suggesting that the presence of glycerol and/or NEM molecules in solution affects the Cu(II) coordination mode. Even more striking is the fact that, if we look at the FT of the EXAFS region of the spectra (Figure 3c), we see that in the sample containing glycerol and NEM a pronounced peak shows up around 3.3 Å, which is absent in the FT of the spectrum of Cu(II) in pure water.

That such a peak is not visible in the absence of NEM is confirmed by the data reported in the right panel of Figure 4, where we compare the FT of the EXAFS region of the spectrum of the S_2 sample (blue curve) with that of a system consisting of 2 mM $CuSO_4$ in a 50% (v/v) glycerol solution and no NEM (purple curve).

An important question that needs to be addressed at this point is whether radiation damage, which is certainly an issue for Cu[1,9,47,48] especially in the presence of glycerol,[2] can be held responsible for the existence of the FT peak visible in Figure 3c showing the data of the S_2 system (blue curve). The answer is that the peak shows up irrespective of the relative amount of the Cu(II) and Cu(I) species mixture that could be present in the sample because of Cu(II) → Cu(I) reduction. This statement is supported by the spectral data we acquired on a sample consisting of 2 mM Cu in a 50% (v/v) glycerol solution (and no NEM). As expected, we find that Cu reduction appears to be significant in the presence of glycerol (similarly to what was found in ref 2), as it is witnessed by presence of the clear pre-edge feature typical of Cu(I) formation (see the purple curve in the left panel of Figure 4), which is absent in the case of Cu in pure water (green curve in Figure 3a). Nevertheless, in the absence of NEM one finds that the peak in the FT around 3.3 Å is absent (see the purple curve in the right panel of Figure 4), just as it is absent in the spectrum of Cu in pure water (green curve in Figure 3c). We are led to conclude that the peak in the FT of S_2 should be ascribed to some ordered structure around the absorber to which both NEM and glycerol contribute.

Fit to XAS Data. Fits to XAS data are obtained making use of the EXCURV98 software package.[24] In order to limit the number of free parameters in the fitting procedure, we have used the so-called constrained refinement method[49] in which molecules made of covalently bound atoms, such as glycerol and NEM, are treated as rigid bodies and only the distance of the nearest atom of each molecule from the metal (leading atom) and possibly the tilt angle of the whole molecule with respect to the vector joining the leading atom to the metal are treated as fitting parameters. The remaining atoms of each molecule rigidly follow the movement of the leading atom.

Naturally, the S_1 EXAFS data are fitted by using as an initial Cu(II) coordination geometry the one provided by model 1 (i.e., that of Cu in pure water). One finds a good fit with Cu coordinated to six water molecules in an octahedral distorted geometry (consistent with other experimental data and theoretical analysis,[32] leading to an *R*-factor of ∼23%. The comparison between EXAFS data and fit is shown in Figure 2 of the Supporting Information. Structural data are collected in Table 1 of the Supporting Information.

Turning now to the S_2 system, a remarkably good agreement between the experimental and calculated EXAFS spectra is obtained starting from the structural model denoted as model 2 above. The best fit parameters to the S_2 EXAFS data are collected in Table 1. We report the distances from Cu of the first-shell atoms only. In the fitting procedure all the Debye–Waller (DW) factors have been kept fixed, but different values were used for atoms belonging to different shells. In particular, DW factors were taken to be 0.0015 $Å^2$ for atoms belonging to the first shell, 0.002 $Å^2$ for atoms located at a distance between 3 and 4 Å from the absorber, and 0.005 $Å^2$ for atoms located at a distance between 4 and 5 Å.

Table 1. Best Fit Structural Parameters of the Cu(II) Site in the S_2 Sample

first-shell Cu coordinated atoms	distance $r \pm \Delta r$ (Å)
1 N(NEM1)	2.05 ± 0.01
1 N(NEM2)	2.27 ± 0.01
1 O(GLY)	1.94 ± 0.01
1 O(GLY)	2.43 ± 0.01
1 O(H_2O)	1.94 ± 0.01
E_F = 0.2 ± 0.5 eV	
R-factor = 19%	
BVS = 1.8	

As one can see from the left panel of Figure 5, where we compare the experimental EXAFS data with the best fit curve, the agreement with the theoretical spectrum provided by the Cu coordination in model 2 is very satisfactory, giving a pretty good *R*-factor of about 19%. In the right panel of Figure 5 we show that also the characteristic peak at ∼3.3 Å visible in the FT is correctly reproduced.

From the best fit values of the structural parameters reported in Table 1, we conclude that Cu(II) is bound to two NEM molecules through their ring nitrogens, one bidentate glycerol molecule (with two O's lying within a distance of 2.5 Å from Cu), and one O belonging to a water molecule.

A few observations are in order here. The first is that some of the first-shell distances around Cu reported in Table 1 may seem somewhat too large compared to crystal structures of similar compounds. Actually, from a careful search in the CSD data bank[38] we find that this is not so. We give a detailed account of the analysis leading to this conclusion in the Supporting Information.

A second observation is that the kind of Cu–NEM coordination we have found appears to be at odds with the fact that the many different buffers containing a morpholine group studied in the literature have been found to have rather weak interactions with metal ions.[3,50−52]

However, the NEM buffer we used in the present investigation (which is the one regularly provided by TCI, https://www.tcichemicals.com/) was not included in this study. It is also used in XAS and ESR combined experiments,[19] owing to its reported ability of silencing the electron spin resonance of Cu(II) ions.[11,13] We give a more thorough discussion of the situation in the Supporting Information.

In Figure 6 we sketch the best fit Cu(II) atomic coordination geometry including all the atoms belonging to molecules having at least one atom located within 5 Å from Cu. For completeness we also provide the bond valence sum (BVS) value associated with the Cu(II) atomic environment of Table 1. We find BVS ∼ 1.8, a value well compatible with a doubly ionized Cu ion. [BVS is a coordination chemistry parameter designed to estimate the validity of a proposed coordination of a metal ion given its oxidation state.[53] The BVS should correspond to the (nominal) ion oxidation state. BVS is calculated as the sum of individual bond valences, according to the formula $V = \sum_i v_i$, with

https://dx.doi.org/10.1021/acs.jpcc.0c08676
J. Phys. Chem. C XXXX, XXX, XXX−XXX

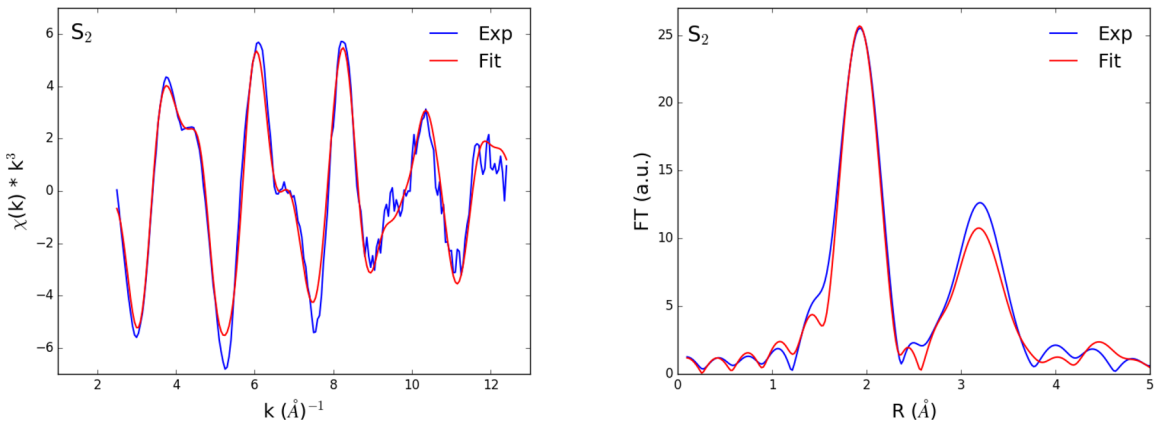

Figure 5. Best fit of model 2 (red curve) vs experimental S_2 data (blue curve). Left panel: EXAFS data. Right panel: Fourier transform of EXAFS data.

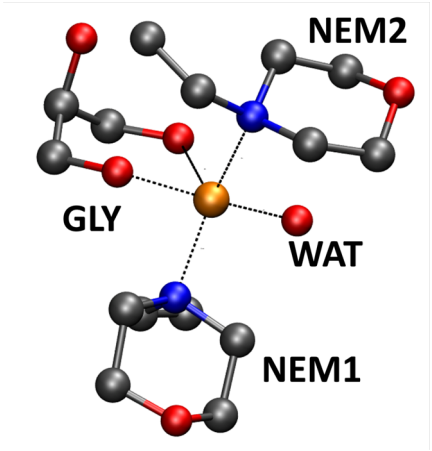

Figure 6. Sketch of the Cu(II) coordination geometry that comes from the best fit of the S_2 EXAFS spectrum. Cu(II) is coordinated to two NEM molecules through their ring nitrogens, one bidentate glycerol molecule (with two O's lying within a distance of 2.5 Å from Cu), and one O belonging to a water molecule. Color code is as in Figure 2. As usual, the geometric parameters of H atoms are not among the fitting parameters and therefore H atoms are not shown.

$$v_i = \exp\left(\frac{R_{0i} - R_i}{b}\right)$$

R_i is the observed bond length of atom i, R_{0i} is a tabulated set of parameters representing the ideal bond length of the relevant pairs of atoms, and b is an empirical constant. Coordination geometries whose BVS values do not differ from the ideal one for more than about 10% are considered good models.]

We note that the Cu−NEM binding mode we have identified displays a rearrangement of Cu−N bonds, with one Cu−N(NEM) bond axial with respect to the NEM morpholine ring. This rearrangement is accompanied by a chair inversion in the same morpholine ring. The final geometry resembles that of the crystal structure of (bis-piperidine-*N*)−Cu(I) complex reported in the CSD under the code CCDC 245157 (BEVLUK).[54,55]

Model 3, where glycerol but not NEM is present, does not provide, instead, a satisfactory representation of the experimental spectrum (giving an *R*-factor of ∼40%). In particular, it is unable to reproduce the peculiar feature at ∼3.3 Å visible in the FT of the EXAFS region (data not shown).

As a further support to the above analysis, we report in the Supporting Information the results of a thorough search in the CSD (distribution 2020[38]) of other possible sets of ordered atoms located in the second Cu coordination shell that could possibly be responsible for the appearance of the 3.3 Å bump in the FT of the EXAFS region of the spectrum. The exhaustive search we present does not lead to the identification of any such organized atomic structure (see the Supporting Information for details).

The peculiar structure of the Cu site we have identified is especially noteworthy in view of the fact that cryoprotectants (such as glycerol) and buffers (such as NEM) are largely employed in most of the experiments in biological inorganic chemistry (such as XAS, ESR, and binding thermodynamics). In particular, buffers containing both NEM and glycerol are widely used in ESR experiments (see for instance ref 14). It is quite interesting to notice that the structural results of the analysis of our EXAFS data we have carried out may offer an explanation for the quenching of the ESR signal of aqueous Cu(II) species reported in refs 13 and 14. [Naturally quenching of the ESR signal can occur also for other reasons, for instance, as suggested in ref 16, because of the formation of silent $[Cu(OH)_2]_n$ diamagnetic species. Discussing this issue is, however, beyond the scope of the present work.] In fact, a quantum mechanical calculation of the Cu spin density distribution over the Cu coordination site confirms that the spin density tends to be spread among the nearest ligands and in particular over the far O(NEM) atom.

This conclusion comes from a comparative *first principle* calculation of the spin density distribution over the Cu coordination site in models 1, 2, and 3. We see from the numbers reported in the second column of Table 2 that the spin density over Cu is minimal in the case of our best fit model 2. We interpret a lower value of μ_z as due to the fact that spin is pushed away from Cu by the presence of the two Cu−

Table 2. Magnetization, μ_z, on the Cu Site Evaluated by Projecting KS states on the Cu Atomic Orbitals of DFT Relaxed Configurations

model	μ_z(Cu) (Bohr magneton)
1	0.67
2	0.46
3	0.66

https://dx.doi.org/10.1021/acs.jpcc.0c08676
J. Phys. Chem. C XXXX, XXX, XXX−XXX

N(NEM) bonds more strongly than when NEM is absent. The effect of the presence of NEM is also neatly visible in Figure 7,

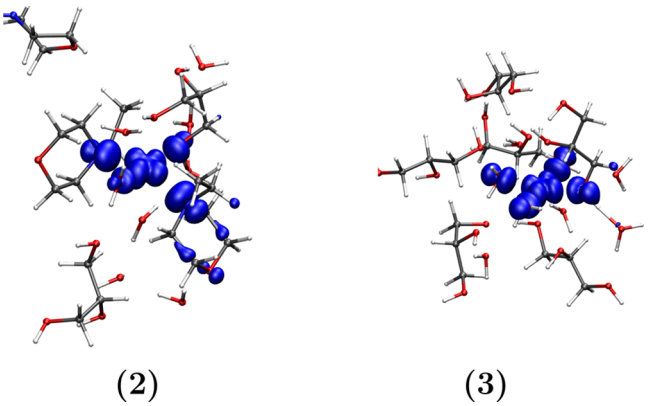

Figure 7. Spin density (difference between spin-up and spin-down components as a function of position in real space) of models 2 and 3. We plot in blue the spin density isosurface at 0.002. Atom color code is as in Figure 2.

where we compare the spin density isosurface (taken at a value equal to 0.002) of model 2 (left panel) and with that of model 3 (right panel). It is seen that in model 2 the spin density is spread along the NEM−Cu ligand.

CONCLUSIONS

In this work we have compared XAS data of Cu in water in the presence of glycerol cryoprotectant and *N*-ethylmorpholine (NEM) buffer (S_2 sample) with models of Cu coordination in two different solution conditions, namely, in a glycerol/water matrix in the presence of NEM (model 2) and in the absence of NEM (model 3).

The careful analysis of the XAS data we have carried out leads to the conclusion that Cu ions in solution with NEM and glycerol display a well-defined relative geometrical arrangement that yields appreciable contributions to the XAS spectrum also from atoms normally considered as "second-shell" atoms. Second-shell atoms can contribute only when they are in stable positions (otherwise disorder kills the signal) or, in other words, when they belong to molecules directly coordinated to the absorber. Second-shell contributions are normally considered the hallmarks of the metal coordinating to the protein once the former is added in solution. This is what happens when dealing with IDPs that, at variance with the situation one encounters in the case of the preorganized metal binding sites of metalloproteins, show weaker metal affinity and high coordination flexibility.

From the structural point of view the Cu−NEM coordination mode we have found is characterized by a conformational change in one of the two NEM ligand molecules with respect to the arrangement of the morpholine rings in the original structure of the ACMRCU10 complex. This conformational change is favored by the kind of environment present in the solvated phase, while it would be hindered by crystal packing. The structure we propose is also consistent with the reduction of the spin density over Cu seen in ESR spectroscopy[13,14] that we have confirmed by a direct quantum mechanical computation.

ASSOCIATED CONTENT

Supporting Information

The Supporting Information is available free of charge at https://pubs.acs.org/doi/10.1021/acs.jpcc.0c08676.

Structural model of S_1 (PDB)
Structural model of S_2 (PDB)
pH of sample at increasing values of glycerol concentration; XANES data of S_1 corrected for self-absorption effects, superimposed to uncorrected data and to data of 2 mM $CuSO_4$ in water; S_1 scans acquired in sample points located 400 μm from each other; S_2 scans acquired in sample points located 300 or 400 μm from each other; best fit of theoretical and experimental S_1 EXAFS data; best fit structural parameters of Cu(II) site in S_1 sample; FT of EXAFS region of samples S_1 and S_2 extended up to 8 Å (PDF)

AUTHOR INFORMATION

Corresponding Author

Silvia Morante − *Universitá di Roma Tor Vergata, 00133 Roma, Italy; INFN, Sezione di Roma Tor Vergata, 00133 Roma, Italy;* orcid.org/0000-0002-3913-5733; Phone: +39 3402533713; Email: silvia.morante@roma2.infn.it

Authors

Giovanni La Penna − *CNR - Istituto di chimica dei composti organometallici, 50019 Sesto Fiorentino, Italy; INFN, Sezione di Roma Tor Vergata, 00133 Roma, Italy;* orcid.org/0000-0002-8619-4867

Fabrizio Machetti − *CNR - Istituto di chimica dei composti organometallici, 50019 Sesto Fiorentino, Italy; Dipartimento di chimica "Ugo Schiff", Universitá di Firenze, 50019 Sesto Fiorentino, Italy*

Olivier Proux − *Observatoire des Sciences de l'Univers de Grenoble, UMS 832 CNRS−Université Grenoble Alpes, 38041 Grenoble, France*

Giancarlo Rossi − *Universitá di Roma Tor Vergata, 00133 Roma, Italy; INFN, Sezione di Roma Tor Vergata, 00133 Roma, Italy; Centro Fermi - Museo Storico della Fisica e Centro Studi e Ricerche E. Fermi, 00184 Roma, Italy*

Francesco Stellato − *Universitá di Roma Tor Vergata, 00133 Roma, Italy; INFN, Sezione di Roma Tor Vergata, 00133 Roma, Italy*

Complete contact information is available at: https://pubs.acs.org/10.1021/acs.jpcc.0c08676

Notes

The authors declare no competing financial interest.

ACKNOWLEDGMENTS

Numerical calculations have been made possible owing to a CINECA−INFN agreement, providing access to resources on MARCONI at CINECA. This work was partially supported by the BIOPHYS initiative (INFN, Italy) and by INAIL (Italy) through the BRiC 2016 ID17/2016 grant. We also acknowledge partial financial support from the MIUR (Italy) PRIN-201744NR8S project.

REFERENCES

(1) George, G. N.; Pickering, I. J.; Pushie, M. J.; Nienaber, K.; Hackett, M. J.; Ascone, I.; Hedman, B.; Hodgson, K. O.; Aitken, J. B.;

(1) Levina, A.; et al. X-ray-induced photo-chemistry and X-ray absorption spectroscopy of biological samples. *J. Synchrotron Radiat.* **2012**, *19*, 875−886.

(2) Nienaber, K. H.; Pushie, M. J.; Cotelesage, J. J.; Pickering, I. J.; George, G. N. Cryoprotectants severely exacerbate X-ray-induced photoreduction. *J. Phys. Chem. Lett.* **2018**, *9*, 540−544.

(3) Ferreira, C. M.; Pinto, I. S.; Soares, E. V.; Soares, H. M. (Un) suitability of the use of pH buffers in biological, biochemical and environmental studies and their interaction with metal ions-a review. *RSC Adv.* **2015**, *5*, 30989−31003.

(4) Thompson, R. F.; Walker, M.; Siebert, C. A.; Muench, S. P.; Ranson, N. A. An introduction to sample preparation and imaging by cryo-electron microscopy for structural biology. *Methods* **2016**, *100*, 3−15.

(5) Churion, K. A.; Bondos, S. E. *Intrinsically Disordered Protein Analysis*; Springer: 2012; pp 415−427.

(6) Rózga, M.; Protas, A. M.; Jabłonowska, A.; Dadlez, M.; Bal, W. The Cu(ii) complex of Aβ40 peptide in ammonium acetate solutions. Evidence for ternary species formation. *Chem. Commun.* **2009**, 1374−1376.

(7) Nagaj, J.; Stokowa-Sołtys, K.; Kurowska, E.; Fraczyk, T.; Jeżowska-Bojczuk, M.; Bal, W. Revised Coordination Model and Stability Constants of Cu(II) Complexes of Tris Buffer. *Inorg. Chem.* **2013**, *52*, 13927−13933.

(8) Bin, Y.; Jiang, Z.; Xiang, J. Side Effect of Tris on the Interaction of Amyloid β-peptide with Cu2.: Evidence for Tris-Aβ-Cu2. Ternary Complex Formation. *Appl. Biochem. Biotechnol.* **2015**, *176*, 56−65.

(9) Summers, K. L.; Schilling, K. M.; Roseman, G.; Markham, K. A.; Dolgova, N. V.; Kroll, T.; Sokaras, D.; Millhauser, G. L.; Pickering, I. J.; George, G. N. X-ray Absorption Spectroscopy Investigations of Copper(II) Coordination in the Human Amyloid β Peptide. *Inorg. Chem.* **2019**, *58*, 6294−6311.

(10) Drew, S. C.; Noble, C. J.; Masters, C. L.; Hanson, G. R.; Barnham, K. J. Pleomorphic Copper Coordination by Alzheimer's Disease Amyloid-β Peptide. *J. Am. Chem. Soc.* **2009**, *131*, 1195−1207.

(11) Shin, B.-k.; Saxena, S. Substantial Contribution of the Two Imidazole Rings of the His13-His14 Dyad to Cu(II) Binding in Amyloid-β(1−16) at Physiological pH and Its Significance. *J. Phys. Chem. A* **2011**, *115*, 9590−9602.

(12) Silva, K. I.; Michael, B. C.; Geib, S. J.; Saxena, S. ESEEM Analysis of Multi-Histidine Cu(II)-Coordination in Model Complexes, Peptides, and Amyloid-β. *J. Phys. Chem. B* **2014**, *118*, 8935−8944.

(13) Jun, S.; Gillespie, J. R.; Shin, B.-k.; Saxena, S. The Second Cu(II)-Binding Site in a Proton-Rich Environment Interferes with the Aggregation of Amyloid-β(1−40) into Amyloid Fibrils. *Biochemistry* **2009**, *48*, 10724−10732.

(14) Shin, B.-k.; Saxena, S. Insight into Potential Cu(II)-Binding Motifs in the Four Pseudorepeats of Tau Protein. *J. Phys. Chem. B* **2011**, *115*, 15067−15078.

(15) Syme, C. D.; Nadal, R. C.; Rigby, S. E. J.; Viles, J. H. Copper Binding to the Amyloid-β (Aβ) Peptide Associated with Alzheimer's Disease: Folding, Coordination Geometry, pH Dependence, Stoichiometry, and Affinity of Aβ-(1−28): Insights From a Range of Complementary Spectroscopic Techinques. *J. Biol. Chem.* **2004**, *279*, 18169−18177.

(16) Aronoff-Spencer, E.; Burns, C. S.; Avdievich, N. I.; Gerfen, G. J.; Peisach, J.; Antholine, W. E.; Ball, H. L.; Cohen, F. E.; Prusiner, S. B.; Millhauser, G. L. Identification of the Cu2. Binding Sites in the N-Terminal Domain of the Prion Protein by EPR and CD Spectroscopy. *Biochemistry* **2000**, *39*, 13760−13771.

(17) Stellato, F.; Spevacek, A.; Proux, O.; Minicozzi, V.; Millhauser, G.; Morante, S. Zinc modulates copper coordination mode in prion protein octa-repeat subdomains. *Eur. Biophys. J.* **2011**, *40*, 1259−1270.

(18) Stellato, F.; Minicozzi, V.; Millhauser, G. L.; Pascucci, M.; Proux, O.; Rossi, G. C.; Spevacek, A.; Morante, S. Copper-zinc cross-modulation in prion protein binding. *Eur. Biophys. J.* **2014**, *43*, 631−642.

(19) de Santis, E.; Minicozzi, V.; Proux, O.; Rossi, G.; Silva, K. I.; Lawless, M. J.; Stellato, F.; Saxena, S.; Morante, S. Cu(II)- Zn(II) Cross-Modulation in Amyloid-Beta Peptide Binding: An X-ray Absorption Spectroscopy Study. *J. Phys. Chem. B* **2015**, *119*, 15813−15820.

(20) Stellato, F.; Chiaraluce, R.; Consalvi, V.; de Santis, E.; la Penna, G.; Proux, O.; Rossi, G.; Morante, S. Dealing with Cu reduction in X-ray Absorption Spectroscopy experiments. *Metallomics* **2019**, *11*, 1401−1410.

(21) Proux, O.; Biquard, X.; Lahera, E.; Menthonnex, J.; Prat, A.; Ulrich, O.; Soldo, Y.; Trévisson, P.; Kapoujyan, G.; Perroux, G.; et al. FAME: A new beamline for X-ray absorption investigations of very-diluted systems of environmental, material and biological interests. *Phys. Scr.* **2005**, *2005*, 970.

(22) Ravel, B.; Newville, M. ATHENA, ARTEMIS, HEPHAESTUS: data analysis for X-ray absorption spectroscopy using IFEFFIT. *J. Synchrotron Radiat.* **2005**, *12*, 537−541.

(23) Newville, M.; Līviņš, P.; Yacoby, Y.; Rehr, J.; Stern, E. Near-edge X-ray-absorption fine structure of Pb: A comparison of theory and experiment. *Phys. Rev. B: Condens. Matter Mater. Phys.* **1993**, *47*, 14126.

(24) Binsted, N.; Gurman, S.; Campbell, J. *Daresbury Laboratory EXCURV98 Program*; CLRC Daresbury: Warrington, U.K., 1998.

(25) la Penna, G.; Minicozzi, V.; Morante, S.; Rossi, G. C.; Stellato, F. A first-principle calculation of the XANES spectrum of Cu2+ in water. *J. Chem. Phys.* **2015**, *143*, 124508−124515.

(26) Towey, J. J.; Soper, A. K.; Dougan, L. What happens to the structure of water in cryoprotectant solutions? *Faraday Discuss.* **2014**, *167*, 159−176.

(27) Akinkunmi, F. O.; Jahn, D. A.; Giovambattista, N. Effects of Temperature on the Thermodynamic and Dynamical Properties of Glycerol-Water Mixtures: A Computer Simulation Study of Three Different Force Fields. *J. Phys. Chem. B* **2015**, *119*, 6250−6261.

(28) Humphrey, W.; Dalke, A.; Schulten, K. VMD visual molecular dynamics. *J. Mol. Graphics* **1996**, *14*, 33−38. http://www.ks.uiuc.edu/Research/vmd.

(29) Jorgensen, W. L.; Chandrasekhar, J.; Madura, J. D.; Impey, R. W.; Klein, M. J. Comparison of simple potential functions for simulating liquid water. *J. Chem. Phys.* **1983**, *79*, 926−935.

(30) Chelli, R.; Procacci, P.; Cardini, G.; Califano, S. Glycerol condensed phases. Part II. A molecular dynamics study of the conformational structure and hydrogen bonding. *Phys. Chem. Chem. Phys.* **1999**, *1*, 879−885.

(31) Plimpton, S. Fast Parallel Algorithms for Short-Range Molecular Dynamics. *J. Comput. Phys.* **1995**, *117*, 1−19. https://lammps.sandia.gov/.

(32) la Penna, G.; Minicozzi, V.; Morante, S.; Rossi, G.; Stellato, F. A first-principle calculation of the XANES spectrum of Cu^{2+} in water. *J. Chem. Phys.* **2015**, *143*, 124508.

(33) Liao, Q.; Kamerlin, S. C. L.; Strodel, B. Development and application of a nonbonded Cu^{2+} model that includes the Jahn-Teller effect. *J. Phys. Chem. Lett.* **2015**, *6*, 2657−2662.

(34) Pang, Y.-P. Successful molecular dynamics simulation of two zinc complexes bridged by a hydroxide in phosphotriesterase using the cationic dummy atom method. *Proteins: Struct., Funct., Genet.* **2001**, *45*, 183−189.

(35) Furlan, S.; Hureau, C.; Faller, P.; la Penna, G. Modeling the Cu^{+} Binding in the 1−16 Region of the Amyloid-β Peptide Involved in Alzheimer's Disease. *J. Phys. Chem. B* **2010**, *114*, 15119−15133.

(36) la Penna, G.; Hureau, C.; Andreussi, O.; Faller, P. Identifying, by First-Principles Simulations, Cu[Amyloid-β] Species Making Fenton-Type Reactions in Alzheimer's Disease. *J. Phys. Chem. B* **2013**, *117*, 16455−16467.

(37) Duarte, F.; Bauer, P.; Barrozo, A.; Amrein, B. A.; Purg, M.; Åqvist, J.; Kamerlin, S. C. L. Force Field Independent Metal Parameters Using a Nonbonded Dummy Model. *J. Phys. Chem. B* **2014**, *118*, 4351−4362.

https://dx.doi.org/10.1021/acs.jpcc.0c08676
J. Phys. Chem. C XXXX, XXX, XXX−XXX

(38) Allen, F. H. Cambridge Structural Database System, Cambridge Crystallographic Data. *Acta Crystallogr., Sect. B: Struct. Sci.* **2002**, *B58*, 380−388.
(39) Battaglia, L.; Corradi, B.; Palmieri, G. Bisacetatobismorpholinecopper (II) dihydrate C12H28CuN2O8. *Cryst. Struct. Commun.* **1973**, *2*, 523−525.
(40) https://www.ccdc.cam.ac.uk/structures/Search?Ccdcid=ACMRCU10&DatabaseToSearch=Published.
(41) Jorgensen, W. L.; Maxwell, D. S.; Tirado-Rives, J. Development and Testing of the OPLS All-Atom Force Field On Conformational Energetics and Properties of Organic Liquids. *J. Am. Chem. Soc.* **1996**, *118*, 11225−11236.
(42) Selvåg, J.; Kuznetsova, T.; Kvamme, B. Molecular dynamics study of surfactant-modified water-carbon dioxide systems. *Mol. Simul.* **2018**, *44*, 128−136.
(43) Giannozzi, P.; Baroni, S.; Bonini, N.; Calandra, M.; Car, R.; Cavazzoni, C.; Ceresoli, D.; Chiarotti, G. L.; Cococcioni, M.; Dabo, I.; et al. QUANTUM ESPRESSO: a modular and open-source software project for quantum simulations of materials. *J. Phys.: Condens. Matter* **2009**, *21*, 395502.
(44) Vanderbilt, D. Soft Self-Consistent Pseudopotentials in a Generalized Eigenvalue Formalism. *Phys. Rev. B: Condens. Matter Mater. Phys.* **1990**, *41*, 7892−7895.
(45) Perdew, J. P.; Burke, K.; Ernzerhof, M. Generalized Gradient Approximation Made Simple. *Phys. Rev. Lett.* **1996**, *77*, 3865−3868.
(46) Andreussi, O.; Dabo, I.; Marzari, N. Revised Self-Consistent Continuum Solvation in Electronic-Structure Calculations. *J. Chem. Phys.* **2012**, *136*, 064102.
(47) McDonald, A.; Pushie, M. J.; Millhauser, G. L.; George, G. N. New insights into metal interactions with the prion protein: EXAFS analysis and structure calculations of copper binding to a single octarepeat from the prion protein. *J. Phys. Chem. B* **2013**, *117*, 13822−13841.
(48) Pushie, M. J.; Nienaber, K. H.; McDonald, A.; Millhauser, G. L.; George, G. N. Combined EXAFS and DFT Structure Calculations Provide Structural Insights into the 1:1 Multi-Histidine Complexes of CuII, CuI and ZnII with the Tandem Octarepeats of the Mammalian Prion Protein. *Chem. - Eur. J.* **2014**, *20*, 9770.
(49) Binsted, N.; Strange, R. W.; Hasnain, S. S. Constrained and restrained refinement in EXAFS data analysis with curved wave theory. *Biochemistry* **1992**, *31*, 12117−12125.
(50) Soares, H. M.; Conde, P. C.; Almeida, A. A.; Vasconcelos, M. T. S. Evaluation of n-substituted aminosulfonic acid pH buffers with a morpholinic ring for cadmium and lead speciation studies by electroanalytical techniques. *Anal. Chim. Acta* **1999**, *394*, 325−335.
(51) Soares, H. M.; Pinho, S. C.; Barros, M. G. R. Influence of N-substituted aminosulfonic acids with a morpholinic ring pH buffers on the redox processes of copper or zinc ions: a contribution to speciation studies. *Electroanalysis* **1999**, *11*, 1312−1317.
(52) Mash, H. E.; Chin, Y.-P.; Sigg, L.; Hari, R.; Xue, H. Complexation of copper by zwitterionic aminosulfonic (good) buffers. *Anal. Chem.* **2003**, *75*, 671−677.
(53) Wood, R. M.; Palenik, G. J. Bond valence sums in coordination chemistry. A simple method for calculating the oxidation state of cobalt in complexes containing only Co- O bonds. *Inorg. Chem.* **1998**, *37*, 4149−4151.
(54) Näther, C.; Beck, A. Chlorobis(piperidine-*κN*)copper(I). *Acta Crystallogr., Sect. E: Struct. Rep. Online* **2004**, *60*, m1008−m1009.
(55) https://www.ccdc.cam.ac.uk/structures/Search?Ccdcid=CCDC%20BEVLUK&DatabaseToSearch=Published.

https://dx.doi.org/10.1021/acs.jpcc.0c08676
J. Phys. Chem. C XXXX, XXX, XXX−XXX